Amorphous Calcium Carbonate (ACC) in *fresco* mural paintings

Núria Oriols[1,2], Nati Salvadó[1*], Trinitat Pradell[3], Salvador Butí[1]

1. Departament d'Enginyeria Química. Universitat Politècnica de Catalunya·BarcelonaTech (UPC). EPSEVG. Av. Víctor Balaguer s/n, 08800 Vilanova i la Geltrú, Barcelona
2. Museu Nacional d'Art de Catalunya, Parc de Montjuïc, 08038 Barcelona
3. Departament de Física, Centre de Recerca en Ciencia i Enginyeria Multiescala de Barcelona. Universitat Politècnica de Catalunya·BarcelonaTech (UPC). Campus Diagonal Besós, Av. Eduard Maristany, 10-14 08019 Barcelona

*corresponding author:
E-mail address: nativitat.salvado@upc.edu

Keywords: carbonation, amorphous calcium carbonate, fresco technique, mural painting

ABSTRACT

A *fresco* painting has a calcium carbonate binder produced as result of the carbonation process of a lime paste. The reaction environmental conditions are similar to those of bio-mineral formation where an amorphous calcium carbonate (ACC) phase has been found to be the precursor of other $CaCO_3$ polymorphs following the sequence: hydrated ACC, anhydrous ACC, vaterite, aragonite, and, finally, stable calcite. In order to determine whether ACC is also formed during the *fresco* drying process, as well as, the final surface calcium carbonate phases present, a series of laboratory mock-ups, replicating as close as possible each of the paint strata and submitted to the same atmospheric conditions have been designed and studied. The results indicate that the continuous supply of water and reagents by the lime and sand mortar promote the ACC formation even at the completion of water evaporation and that the high pH of the medium does not favour the formation of calcium carbonate polymorphs other than calcite. In fact, the results demonstrate that the presence of an ACC layer in the mural painting surface confirms that the original painting technique used was *fresco*. Finally, the presence of an ACC layer is important for stablishing adequate cleaning (the solubility of hydrated ACC is superior to those of calcite) and conservation protocols (ACC is susceptible to suffer dehydration) for the *fresco* paintings.

1. INTRODUCTION

A *fresco* painting has a calcium carbonate binder produced as result of a carbonation process. Consequently, in-depth studies of the carbonation process are essential for establishing adequate strategies for the *fresco* preservation.

The process of biominerals carbonation, as well as of lime mortars drying have been described elsewhere [1,2]. It is known that the water retained in the surface pores plays

a key role in the reaction, and that, the solution supersaturation determines the $CaCO_3$ nucleation rate and crystal growth [3,4]. However, there are still unknown aspects with regard to the materials nature and distribution during the *fresco* drying and subsequent carbonation process. In particular, the relevance during the drying process of the layered structure characteristic of a *fresco* painting, which includes a surface film, a stratum with pigment particles and a layer resulting from the reaction between the mortar and the chromatic layer, is still unknown.

Nevertheless, the reaction environmental conditions (T, P and CO_2 concentration) are similar to those of bio-mineral formation. Under supersaturation conditions, an amorphous calcium carbonate (ACC) phase is found to be the precursor of other $CaCO_3$ polymorphs [5,6] in biominerals and biomimetic materials. ACC is widely present and has influence in the structure, namely stiffens the exoskeletal cuticle in calcareous biominerals such us sea urchin spines and mollusc shells. Moreover, most biogenic ACC deposits that are stable in vivo are also stable when extracted from the organism. Finally, biogenic ACC can be classified as either stable or transient, where the stable form is hydrated (with approximate composition $CaCO_3{:}H_2O$) and the transient form anhydrous [7,8].

Under supersaturation conditions, carbonation has been described as a continuous process; it starts with the formation of a dense liquid, which evolves towards hydrated ACC, then into progressively less hydrated structures and finally into anhydrous ACC. It is believed that in the dense liquid stable pre-nucleation clusters aggregate forming the ACC nanoparticles. These pre-nucleation clusters have been described as dynamic associations of Ca^{2+} and CO_3^{2-} ions or $CaCO_3^{o}$ (aq) ionic pairs forming lineal chains, rings or branches where the water remains as integrated part if the disordered structure [9,10]. Other authors, on the contrary, defend that the crystalline growth of calcium carbonate might also be the result of ions addition following the classic nucleation and growth mechanism [11].

In general, the carbonation process of calcium hydroxide follows the sequence: hydrated ACC, anhydrous ACC, vaterite, aragonite, and, finally, stable calcite [12-14]. In order to determine if this sequence of phases is also present during the *fresco* drying process and which are the final surface calcium carbonate phases present, a series of laboratory *fresco* mock-ups have been designed. The mock-ups, replicating as close as possible each of the paint strata and submitted to the same atmospheric conditions (room temperature of 20±2 ^{o}C, relative humidity of 50±5 % and a concentration of CO_2 of 665-680 ppm), have been monitored and the reaction compounds identified.

The presence/absence of hydrated ACC is important to design strategies for the conservation of the *fresco* paintings. On the one hand, the solubility of hydrated ACC is superior to those of calcite [15,16], a factor of importance when planning water based cleaning protocols for the *fresco* paintings. On the other hand, hydrated ACC is

susceptible to suffer dehydration [2], which is an important fact on establishing adequate environmental humidity control systems [17,18].

A series of *fresco* mock-ups were made using the raw materials traditionally used. In parallel, a set of calcium hydroxide water solution droplets were also prepared from both, traditional raw materials and reagents. Finally, the carbonation process of both droplets and mock-ups was monitored using optical microscopy (OM) and Field Emission Scanning Electron Microscopy (FESEM) and the reaction compounds formed identified by Fourier Transform Infrared microspectroscopy (μ-FTIR), Raman Spectroscopy and Micro-X-ray Diffraction (micro-XRD).

2. EXPERIMENTAL

The optical images have been obtained with a Reichert-Jung POLYVAR MET Optical Microscope in transmission and reflexion mode (dark field, bright field and polarized light and 50x to 1000x magnification). The samples were carbon-coated to ensure the necessary electrical conductivity for SEM imaging. Secondary Electron images obtained with acceleration voltages between 10 kV and 20 kV by FESEM (Jeol J-7100).

μ-FTIR (SPOTLIGHT 100/Frontier PerkinElmer, MCT detector, 600-4000 cm^{-1}) spectra were obtained in transmission mode from 100x100 μm areas of the samples prepared using a diamond cell. Raman spectra were obtained with a RENISHAW inVia Qontor Raman laser microscope (532 nm, spectroscopic range 2000 to 100 cm^{-1}, which covers de region of interest of the $CaCO_3$ polymorphs). Finally, micro-XRD has been performed at XALOC beamline at the Alba synchrotron (Cerdanyola del Vallès, Barcelona); the low energy <10keV, high brilliance and focused beam 30x7 μm^2 (width x height FWHM) together with the eventually noise-free large-area photon counting detector (Pilatus 6M) provides the necessary requirements for the determination of the crystalline compounds and their distribution in the samples.

In order to obtain the materials traditionally used to produce the *frescos*, a water suspension of the slaked lime putty commonly used by painters and conservators (*Chaux Almox: Chaux grassenpâte*), mainly, $Ca(OH)_2$ (portlandite), was left to age for one year in a partly covered beaker. After one year of aging, three layers formed in the lime putty: (i) a translucent surface film, (ii) an intermediate liquid transparent layer and (iii) a dense white opaque layer on the base. These layers are equivalent to the products traditionally known as (i) lime veil (ii) lime-water and (iii) putty lime or lime paste [17]. The *lime veil* formed on the surface of the lime-water was not removed until the putty lime was to be used for painting or conservation of *frescos*; most probably because it limited the CO_2 diffusion into the lime putty protecting from an earlier carbonation.

A series of drops of 100 and 300 μL aliquots of calcium hydroxide solutions ($Ca(OH)_2$ Merck 1.02047 in H_2O LC-MS quality Panreac 701074) and of lime-water saturated

solutions (200 mL of a suspension of 180 g of slaked lime) were laid over microscope slides and left to dry in contact with the atmosphere (30-60 min at room temperature and pressure).

Little morphological changes and none new structures are detected after 30 days of monitoring the carbonation of lime-water drops, indicating that the absence of water slows down or even stops the process independently of the stage of the process. For this reason, a set of replicas corresponding to the different stages of the carbonation process were prepared. Forcing the extraction of the water from the drop base with cellulose fibre the initial drying stage was also replicated.

Lime-water drops mixed with various blue pigments, lapis lazuli (Kremer 10540) and aerinite a natural rock from *Les Avellanes i Santa Linya* (Noguera county, Catalunya) and red pigments, hematite (Kremer 48651), Terra Pozzuoli (Kremer 41550) and vermilion (Kremer 42000) were also prepared.

Mock-ups of the *fresco* painting applied over a fresh commercial lime putty mortar have also been prepared to replicate the long-term evolution of the carbonation process. Contrarily to the glass substrate, the mortar continually supplies water with Ca^{2+} and OH^- ions from the lime paste which contains portlandite, $Ca(OH)_2$ and humidity.

Moreover, a mock-up replicating the stratigraphy and composition of a typical Catalan Romanesque *fresco* was also produced. The mock-up has: two layers (*arriccio* and *intonaco*) of a mortar made of a mixture 1:1 and 3:1 respectively of lime putty and sand of various grain sizes. The mortar layers were applied over a wet wooden case (18.5 x 48.5 cm made with two tongue and groove joints). Finally, the pigments mixed with water or lime-water applied over the wet mortar surface (*fresco*) or mixed with a binder (rabbit glue, casein, egg yolk or linseed oil) were applied over the dry mortar surface (*secco*). Mock-ups were prepared from mortars of various thicknesses and with stacks of layers combining *fresco* and *secco* painting.

Finally, in order to proceed to the study of the compounds obtained (i) material was extracted from the surface and at different depths from the inner layers; (ii) surfaces of about 2 mm^2 area were inspected and, (iii) cross sections of various thicknesses of the fragments were prepared.

3. RESULTS AND DISCUSSION

3.1 MONITORIZATION OF THE CARBONATION OF THE DROPLETS

The drops laid over microscope slides show different stages of the nucleation and growth of the calcium carbonate. In this system, the diffusion/dissolution of CO_2 limits the effect of surface porosity which exists in a fresh painting/lime mortar system.

The calcium carbonate polymorph formed depends on the concentration of the $Ca(OH)_2$ solution. Crystalline structures (with birefringence) identified as calcite by μFTIR and Raman spectroscopy are formed at the edge of the $Ca(OH)_2$ diluted water droplets, where the water first evaporates. On the contrary, amorphous structures (without birefringence) are formed in supersaturated lime-water droplets (**Figure 1**).

Thanks to the stillness of the lime-water droplets, we can see how the formation of ACC spherulitic particles initiates from the liquid phase, whose density is probably different than those of the initial solution. The distribution of these particles is similar to the spatial patterns produced upon spinodal decomposition and binodal demixing/nucleation in a liquid-liquid phase separation [9,19,20]. Spherolitic particle aggregates of ACC nanoparticles are observed by transmission and reflection dark field optical microscopy (**Figure 1a,b**) and the ACC nanoparticles (~100nm) are determined by SEM (**Figure 1c**). These aggregates coalesce in the dense liquid phase forming a vitreous like thin film. This process corresponds to the initial steps of the carbonation process. The FTIR spectrum of ACC (**Figure 1d**) shows a shoulder on the main asymmetric ν3 carbonate band (1474 cm^{-1}) and the absence of the ν4 symmetric vibration characteristic of crystalline calcium carbonate phases (713 cm^{-1} calcite, 745 cm^{-1} vaterite and 700/712 cm^{-1} aragonite). It also shows a small band at 1645 cm^{-1} (H–O–H bending), and a broad band between 3200 and 3400 cm^{-1} (O–H stretching), both of which correspond to structural water within ACC. The remaining bands related to the vibrations of the carbonate ions (1417, 1075 and 867 cm^{-1}) are common in both poorly-ordered ACC and crystalline polymorphs.

ACC cannot form in a solution concentrated below saturation, and consequently, following the free-energy landscape of calcium carbonate [21] more insoluble crystalline calcite structures are formed by nucleation and growth instead ACC in the $Ca(OH)_2$ diluted water droplets. Contrarily, in supersaturated solutions, the carbonation process initiates with the formation of hydrated ACC, and this happens both at the edge and at the surface of the droplet, which is the region with the highest concentration of CO_3^{2-} ions. In our experiment, the slow diffusion of CO_2 in water compared to air (diffusion coefficients of CO_2 in water is approximately 10000 times lower than in air [22]) generates a concentration gradient of CO_3^{2-} ions between the surface of the drop and the base which is touching the microscope slide. Moreover, the suspension of polygonal platelets [23] of portlandite, $Ca(OH)_2$, found over the microscope slide in the lime-water droplets act as a continuous source of Ca^{2+} and OH^- ions, which, in our case, contribute to maintain supersaturation.

The ACC spherulitic particles aggregates evolve towards platelets or chain-like structures. Those more hydrated (Type I) coalesce and form iridescent platelets when observed in Bright Field (**Figure 1e**). Chain-like aggregates (Type II) are more opaque and show also more contrast in the SEM images (**Figure 1f,g**). Those chain-like aggregates act as an intermediate phase towards the formation of micrometric

crystallites of an anhydrous polymorph of $CaCO_3$. The broad band at 866 cm^{-1} and the narrow band at 872 cm^{-1} (**Figure 1d**) correspond to the presence of a mixture of type I and type II ACC structures. This splitting of the ν2 vibration indicates the beginning of their crystallisation and partial dehydration [6].

Many papers [2,3,24] explain how once the hydrated ACC is formed it continues the evolution towards anhydrous ACC and more stable crystalline $CaCO_3$ polymorphs. During this process, water is released from the ACC structures and, as a result, the supersaturation locally decreases favouring the dissolution of hydrated ACC and the precipitation of the more anhydrous and insoluble structures. In our experiment, following the carbonation process at the lime-water droplet surface, we can observe (**Figure 1h**) a dissolution-and-reprecipitation process around the individual calcite $CaCO_3$ particles. The H_2O molecules released during the formation of anhydrous $CaCO_3$ phases create a region-free of particles around this isolated calcite particles, at the same time that the shape of the spherical aggregates of hydrated ACC changes into chain-like structures.

Following the process, tridimensional birefringent spherical or dendrite flower-like shaped aggregates (1 to 20 μm) vaterite [25] were formed (**Figure 2a-c**). Those structures transform slowly into calcite crystals (**Figure 2d-f**). Calcite with rhomboidal and scalenohedral crystal habits is formed at the expense of the chain-like spherulitic aggregates; the birefringent crystals are located only in the areas which contain chain-like spherulitic aggregates (more opaque to the light in the polarized transmission image) (**Figure 1i**). As long as water is still present in the lime-water droplet (between 30 minutes and 1 hour), it is possible to see by optical microscopy the morphological changes of the transformation of vaterite into calcite. Once the water has completely evaporated, this process slows down or stops, in fact vaterite is still determined in the Raman spectrum after ten days of its formation (**Figure 2c** shows the splitting of both the ν1 and ν4 peaks characteristic of vaterite and related to two distinct site symmetries for the CO_3^{2-} groups [26]).

At the perimeter of the spherical vaterite growths (10 μm) brilliant halos are observed by optical microscopy. The Raman spectrum from this area show peaks at 984, 1020 and 1060 cm^{-1} related to the presence of HCO_3^- and CO_3^{2-} in solution [27]. The presence of HCO_3^- is due to the reduction of the local pH value resulting from a constant supply of CO_2 that decreases the concentration of OH^- ions; for pH below 9.5, the ion predominant in an open to the atmosphere aqueous system is HCO_3^-.

Tobler et al. [28] have determinate that for pH values of about 10 the formation of vaterite from ACC and its subsequent transformation into calcite are favoured. However, increasing the pH the lifetime of ACC increases, and it transforms directly into small crystallites of calcite. For a range of pH values between 10.6 and 12.7 the structure of ACC gradually changes incorporating OH^- ions into structures of the type

$Ca(CO_3)_{(1-x)}(OH)_{2x}\cdot yH_2O$. They conclude that it is probable that the OH^- ions have some inhibitory effect on the nucleation and growth of vaterite.

For this reason, vaterite is detected in the areas with a higher CO_2 supply such as happens in the translucid *lime veil* formed on the surface of the lime paste/water aged for one year and also at the lime-water/atmosphere interface in the lime water droplet. On the other hand, it also explains why the high alkalinity of the lime paste in the mortars does not favour the formation/stability of vaterite. Monohydrocalcite $CaCO_3\cdot H_2O$, a phase which some authors relate to a transient phase [29,30], has also been determined in the *lime veil* layer. The *lime veil* formed over the lime-water shows birefringent crystalline formations with different morphologies and sizes (1-10 μm). The FTIR spectroscopic analysis shows the presence of calcite and ACC and SR-μXRD analysis shows also the presence of calcite, vaterite and monohydrocalcite (**Figure 2g**). A new intermediate crystalline hydrated phase of calcium carbonate, $CaCO_3\cdot 1/2H_2O$ has been recently proposed [31], but it has not been determined in our materials.

The lime-water droplets mixed with pigments show the same carbonation process monitored in the lime-water droplets -formation of ACC particles, vaterite and, finally, calcite-. The main difference found is that the pigment particles surface provides nucleating centres (heterogeneous nucleation [1,32-34]) and, consequently, the spherulitic particles accumulate in the perimeter of the pigment particles (**Figure 1j**).

3.2 CARBONATION PROCESS IN *FRESCO* PAINTING

Lime mortar replica: The presence of ACC spherical particles is determined on the top layer of a three-year old lime mortar replica (**Figure 3a**). The spectrum shows also the shape characteristic of ACC, with the splitting and broadening of the ν3 asymmetric vibration (1415 and 1470 cm^{-1}) bands. 30 days monitoring the evolution of the carbonation surface of the lime mortar replica shows **(Figure 3b)** a decrease of the intensity of the OH^- stretching vibration band at 3645 cm^{-1} and an increase of the intensity of the CO_3^{2-} group vibrations bands (ν1 symmetric stretching, ν2 asymmetric deformation, ν3 asymmetric stretching and ν4 symmetric deformation).

Decreasing the water released from the structure the transformation rate of the hydrated ACC is reduced [35]. ACC precipitates formed in areas with high levels of supersaturation do not show short-range order. This explains why a stable anisotropic transparent vitreous ACC film forms at the surface (Figure 3a).

Mural painting replica: An ACC film formed by superposed submicrometric planes of spherulitic particles is also formed on the top layer of the *fresco* paint (**Figure 3 c,d,e**). The anisotropy of this fine vitreous ACC film may explain some of the characteristic optical properties of the ***fresco*** painting, such as, the colour saturation and transparency

[36]. Moreover, a continuous layer of spherulitic particles is also observed at the interface *fresco*/*secco* (the *secco* layers were applied some days later than the *fresco*) (**Figure 4**).

Owing to the slow CO_2 diffusion rate in water, a maximum of supersaturation happens at the interface paint layer/atmosphere. Therefore, the carbonation process starts at the interface forming hydrated ACC, the most soluble calcium carbonate phase.

The presence of portlandite causes an ongoing release of Ca^{2+} and OH^- ions in the *fresco* replicas. These ions migrate –dissolved in water- from the inner part of the mortar towards the surface where maintain a constant supersaturation degree, which together with the CO_3^{2-} from dissolved CO_2, not only delay the dissolution of ACC but promote its formation even at the cessation of the water evaporation.

The porous and wet structure of the painting layer and mortar, including the cracks, has direct influence in the CO_2 diffusion/dissolution rate, resulting in a variable carbonate concentration. In fact, $CaCO_3$ precipitates of diverse growth habits are found at different depths (**Figure 3c**). This should be related to the presence of different [Ca^{2+}] and [CO_3^{2-}] concentrations (even far from supersaturation) [3,37]. In fact, the water from the lime paste incorporates CO_2 during the aging process but also the mortar and pigment layers of different porosity can supply CO_2 locally even in areas far from the surface.

Just beneath the surface of the thin ACC film, the carbonation process appears more advanced showing an increased amount of calcite with scalenohedral morphology (**Figure 3d**). Following the cross section, the corresponding SEM images show the presence of interconnected chains of $CaCO_3$ particles. The distribution pattern of these particle chains is similar to the morphologies observed in the lime-water droplets. This chain-like morphology is also observed around the pigment particles in the layers of *fresco* painting, demonstrating the binding ability of the calcium carbonate.

In summary, a few microns thick dense rich in calcium carbonate layer [38] is formed at the surface of the *fresco* paints. This is due to the continuous formation of hydrated ACC and its transformation towards anhydrous crystalline and more stable phases. This layer acts as a barrier to the atmospheric CO_2 diffusion inside the *fresco* and, consequently slows down the carbonation process in the inner areas of painting. The *fresco* mock-ups cross-section shows this Ca accumulation on the top layer related to the film made of spherulitic particles, figures 4b-d.

4. CONCLUSION

Monitoring the drying process of lime-water drops and comparing with the process of carbonation of biogenic systems has provided valuable information about the carbonation process in *fresco* paintings. The carbonation of a *fresco* painting is not a fast process in which calcite is directly formed by reaction of lime with the atmospheric CO_2, but a slow process with several stages depending on $CaCO_3$ supersaturation, and the $Ca(OH)_2$ solution in contact with the CO_2 of the atmosphere.

The carbonation of lime in a *fresco*, at room temperature, pressure and environmental CO_2 concentration, follows the sequence: hydrated ACC, anhydrous ACC and formation of crystalline polymorphs of $CaCO_3$. A kinetically controlled process, in which the more soluble species are first formed with a mechanism similar to those happening in the biogenic systems, is driven by the supersaturated solution in contact with the atmosphere and with the lime of the *fresco* painting.

The lime and sand mortar of a *fresco* painting is a source of water and reagents to the surface layer. During the drying of the *fresco* painting, water is driven by capillarity through the porosity of the materials towards the surface of the painting where evaporation happens carrying water from the mortar to the surface (painting/air interface). At the painting/air interface of the *fresco* the same supersaturation level is maintained a long time due to the continuous supply of water and reagents: carbonate ions from dissolved atmospheric CO_2, and calcium ions from the dissolution of the portlandite platelets. This will promote the ACC formation even at the completion of water evaporation.

In lime mortars (without magnesium ions) the high pH of the medium does not favour the formation of calcium carbonate polymorphs other than calcite: vaterite and aragonite have not been identified in our experiments.

With regard to the difficulties often encountered to ascertain the painting technique used in historical mural paintings (either *fresco* or *secco*), the presence of an ACC layer on the mural painting surface may be an indirect confirmation of the use of *fresco.*

The presence of this ACC layer has important implications with regard to the restoration and conservation protocols used in *fresco* paintings. On the one hand, aqueous cleaning should be taken with care, as the solubility of ACC is higher than those of calcite; on the other hand, and considering the susceptibility of hydrated ACC to transform into anhydrous ACC, control of the environmental humidity conditions should be taken into account to improve the *fresco* paintings conservation.

Acknowledgements:

The project received financial support from MINECO (Spain), grant MAT2016-77753-R and Generalitat de Catalunya, grant 2017 SGR 0042. The μSR-XRD experiments were performed at BL13 XALOC beamline at ALBA Synchrotron Facillity with the collaboration of ALBA staff (proposal 2017092488). We acknowledge the collaboration of Mireia Mestre, chief of Restoration Department of MNAC.

References

[1] N.A.J.M. Sommerdijk, G. de With, Biomimetic $CaCO_3$ mineralization using designer molecules and interfaces, Chem. Rev. 108 (2008) 4499–4550. doi:10.1021/cr078259o.

[2] C. Rodriguez-Navarro, K. Kudłacz, Ö. Cizer, E. Ruiz-Agudo, Formation of amorphous calcium carbonate and its transformation into mesostructured calcite, CrystEngComm. 17 (2015) 58–72. doi:10.1039/c4ce01562b.

[3] Ö. Cizer, K. Van Balen, J. Elsen, D. Van Gemert, Real-time investigation of reaction rate and mineral phase modifications of lime carbonation, Constr. Build. Mater. 35 (2012) 741–751. doi:10.1016/j.conbuildmat.2012.04.036.

[4] Ö. Cizer, C. Rodriguez-Navarro, E. Ruiz-Agudo, J. Elsen, D. Van Gemert, K. Van Balen, Phase and morphology evolution of calcium carbonate precipitated by carbonation of hydrated lime, J. Mater. Sci. 47 (2012) 6151–6165. doi:10.1007/s10853-012-6535-7.

[5] J. Evans, Polymorphs, Proteins, and Nucleation Theory: A Critical Analysis, Minerals. 7 (2017) 62. doi:10.3390/min7040062.

[6] J.H.E. Cartwright, A.G. Checa, J.D. Gale, D. Gebauer, C.I. Sainz-Díaz, Calcium carbonate polyamorphism and its role in biomineralization: How many amorphous calcium carbonates are there?, Angew. Chemie - Int. Ed. 51 (2012) 11960–11970. doi:10.1002/anie.201203125.

[7] L. Addadi, S. Raz, S. Weiner, Taking advantage of disorder: Amorphous calcium carbonate and its roles in biomineralization, Adv. Mater. 15 (2003) 959–970. doi:10.1002/adma.200300381.

[8] F.C. Meldrum, Calcium carbonate in biomineralisation and biomimetic chemistry, Int. Mater. Rev. 48 (2003) 187–224. doi:10.1179/095066003225005836.

[9] R. Demichelis, P. Raiteri, J.D. Gale, D. Quigley, D. Gebauer, Stable prenucleation mineral clusters are liquid-like ionic polymers, Nat. Commun. 2 (2011). doi:10.1038/ncomms1604.

[10] D. Gebauer, M. Kellermeier, J.D. Gale, L. Bergström, H. Cölfen, Pre-nucleation clusters as solute precursors in crystallisation, Chem. Soc. Rev. 43 (2014) 2348–2371. doi:10.1039/c3cs60451a.

[11] K. Henzler, E.O. Fetisov, M. Galib, M.D. Baer, B.A. Legg, C. Borca, J.M. Xto, S. Pin, J.L. Fulton, G.K. Schenter, N. Govind, J.I. Siepmann, C.J. Mundy, T. Huthwelker, † James, J. De Yoreo, Supersaturated calcium carbonate solutions are classical, 2018. http://advances.sciencemag.org/.

[12] R.A. Van Santen, The Ostwald step rule, J. Phys. Chem. 88 (1984) 5768–5769. doi:https://doi.org/10.1021/j150668a002.

[13] A. Navrotsky, Energetic clues to pathways to biomineralization: Precursors, clusters, and nanoparticles, Proc. Natl. Acad. Sci. 101 (2004) 12096–12101. doi:10.1073/pnas.0404778101.

[14] J.D. Rodriguez-Blanco, S. Shaw, L.G. Benning, The kinetics and mechanisms of amorphous calcium carbonate (ACC) crystallization to calcite, via vaterite. Nanoscale. 3 (2011) 265–271. doi:10.1039/c0nr00589d.

[15] M.E.Q. Pilson, M.E.Q. Pilson, Solubility of calcium carbonate, in: An Introd. to Chem. Sea, 2013: pp. 450–452. doi:10.1017/cbo9781139047203.023.

[16] L. Brečević, A.E. Nielsen, Solubility of amorphous calcium carbonate, J. Cryst. Growth. (1989). doi:10.1016/0022-0248(89)90168-1.

[17] P. Mora, L. Mora, P. Philippot, Conservation of wall paintings, Butterworths, London [etc.]: 1984.

[18] F. Piqué and G. Veri, Organic materials in Wall Paintings, The getty Conservation Institute, Los Angeles: 2015

[19] M. Faatz, F. Gröhn, G. Wegner, Amorphous calcium carbonate: Synthesis and potential intermediate in biomineralization, Adv. Mater. 16 (2004) 996–1000. doi:10.1002/adma.200306565.

[20] R. Alert, P. Tierno, J. Casademunt, Formation of metastable phases by spinodal decomposition, Nat. Commun. 7 (2016). doi:10.1038/ncomms13067.

[21] A. V. Radha, T.Z. Forbes, C.E. Killian, P.U.P.A. Gilbert, A. Navrotsky, Transformation and crystallization energetics of synthetic and biogenic amorphous calcium carbonate, Proc. Natl. Acad. Sci. 107 (2010) 16438–16443. doi:10.1073/pnas.1009959107.

[22] K. Van Balen. Carbonation reaction of lime, kinetics at ambient temperature. Cement and Concrete Research 35 (2005) 647-657

[23] K. Elert, C. Rodriguez-Navarro, E.S. Pardo, E. Hansen, O. Cazalla, Lime Mortars for the Conservation of Historic Buildings, Stud. Conserv. 47 (2008) 62. doi:10.2307/1506835.

[24] J. Ihli, W.C. Wong, E.H. Noel, Y.-Y. Kim, A.N. Kulak, H.K. Christenson, M.J. Duer, F.C. Meldrum, Dehydration and crystallization of amorphous calcium carbonate in solution and in air., Nat. Commun. 5 (2014) 3169. doi:10.1038/ncomms4169.

[25] J.P. Andreassen, R. Beck, M. Nergaard, Biomimetic type morphologies of calcium carbonate grown in absence of additives, Faraday Discuss. 159 (2012) 247–261. doi:10.1039/c2fd20056b.

[26] R.U.& A.H.H. Gesa Behrens, Liisa T. Kuhn, Raman Spectra of Vateritic Calcium Carbonatee, Spectrosc. Lett. 28 (1995) 983–995. doi:10.1080/00387019508009934.

[27] T. Geisler, C. Perdikouri, A. Kasioptas, M. Dietzel, Real-time monitoring of the overall exchange of oxygen isotopes between aqueous CO_3^{2-} and H_2O by Raman spectroscopy, Geochim. Cosmochim. Acta. 90 (2012) 1–11. doi:10.1016/j.gca.2012.04.058.

[28] D.J. Tobler, J.D. Rodriguez Blanco, H.O. Sørensen, S.L.S. Stipp, K. Dideriksen, Effect of pH on Amorphous Calcium Carbonate Structure and Transformation, Cryst. Growth Des. 16 (2016) 4500–4508. doi:10.1021/acs.cgd.6b00630.

[29] T. Kimura, N. Koga, Thermal dehydration of monohydrocalcite: Overall kinetics and physico-geometrical mechanisms, J. Phys. Chem. A. 115 (2011) 10491–10501. doi:10.1021/jp206654n.

[30] C.R. Blue, A. Giuffre, S. Mergelsberg, N. Han, J.J. De Yoreo, P.M. Dove, Chemical and physical controls on the transformation of amorphous calcium carbonate into crystalline $CaCO_3$ polymorphs, Geochim. Cosmochim. Acta. 196 (2017) 179–196. doi:10.1016/j.gca.2016.09.004.

[31] Z. Zou, W.J.E.M. Habraken, G. Matveeva, A.C.S. Jensen, L. Bertinetti, M.A. Hood, C. Sun, P.U.P.A. Gilbert, I. Polishchuk, B. Pokroy, J. Mahamid, Y. Politi, S. Weiner, P. Werner, S. Bette, R. Dinnebier, U. Kolb, E. Zolotoyabko, P. Fratzl, A hydrated crystalline calcium carbonate phase: Calcium carbonate hemihydrate, Science (80-.). 363 (2019) 396–400. doi:10.1126/science.aav0210.

[32] J.J. De Yoreo, Principles of Crystal Nucleation and Growth, Rev. Mineral. Geochemistry. 54 (2005) 57–93. doi:10.2113/0540057.

[33] J.J. De Yoreo, A holistic view of nucleation and self-assembly, MRS Bull. 42 (2017) 525–531. doi:10.1557/mrs.2017.143.

[34] L. Brecevic, D. Kralj, ChemInform Abstract: On Calcium Carbonates: From Fundamental Research to Application, ChemInform. 39 (2008). doi:10.1002/chin.200805226.

[35] J. Cavanaugh, M.L. Whittaker, D. Joester, Crystallization kinetics of amorphous calcium carbonate in confinement, Chem. Sci. 10 (2019) 5039–5043. doi:10.1039/c8sc05634j.

[36] K. Lee, W. Wagermaier, A. Masic, K.P. Kommareddy, M. Bennet, I. Manjubala, S.W. Lee, S.B. Park, H. Cölfen, P. Fratzl, Self-assembly of amorphous calcium carbonate microlens arrays, Nat. Commun. 3 (2012). doi:10.1038/ncomms1720.

[37] J. García Carmona, J. Gómez Morales, R. Rodríguez Clemente, Rhombohedral-scalenohedral calcite transition produced by adjusting the solution electrical conductivity in the system $Ca(OH)_2$-CO_2-H_2O, J. Colloid Interface Sci. 261 (2003) 434–440. doi:10.1016/S0021-9797(03)00149-8.

[38] R. Piovesan, C. Mazzoli, L. Maritan, P. Cornale, Fresco and lime-paint: An experimental study and objective criteria for distinguishing between these painting techniques, Archaeometry. 54 (2012) 723–736. doi:10.1111/j.1475-4754.2011.00647.x.

FIGURE CAPTIONS

Figure 1. a) Transmission OM, b) reflexion dark field OM of spherolitic aggregates of ACC nanoparticles. c) SEM images of ACC nanoparticles. d) µ-FTIR spectra of (TOP) amorphous calcium carbonate (ACC) from a lime water drop, (BOTTOM) evolution from portlandite to ACC and spectra of ν2 vibration band when both type I and type II of ACC are present (IN THE BOX). e) Transmission OM, f and g) SEM images of type I and type II ACC. h) Dissolution of hydrated ACC and precipitation of more anhydrous and insoluble structures. i) Transmission polarized OM images of chain spherulitic aggregates and birrefringent calcite crystals. j) OM image from the carbonation process of a drop of lapis-lazuli in lime-water.

Figure 2. a) and d) OM image, b) and e) SEM image, c) and f) Raman spectra of vaterite and calcite respectively in lime water drops. g) SR-µXRD pattern from the lime veil showing the presence of calcite, vaterite and monohydrocalcite (signal magnification is represented by a dashed line).

Figure 3. a) SEM images of spherical particles of ACC on the top mortar. b) Infrared spectra of the 28 days evolution (grey line to black line) of the carbonation reaction of the surface layer of a mortar. c) Scheme of the layer sequence of a fresco mural painting: n1, n2 fresco paint and n3, n4 mortar layers. d) SEM image of superposed submicrometric planes of spherulitic particles. e) SEM images of spherical particles of ACC on the top layer (n1) of a fresco, scalenohedral structures below the ACC layer (top of n2) and chain-like morphology of calcium carbonate in the inner mortar layer (n4).

Figure 4. a) Fragment of a *fresco* paint mock-up (–hematite- iron oxide red pigment). b) top layer with spherical aggregates of c) hydrated ACC nanoparticles and d) superposed submicrometric planes of spherulitic particles.

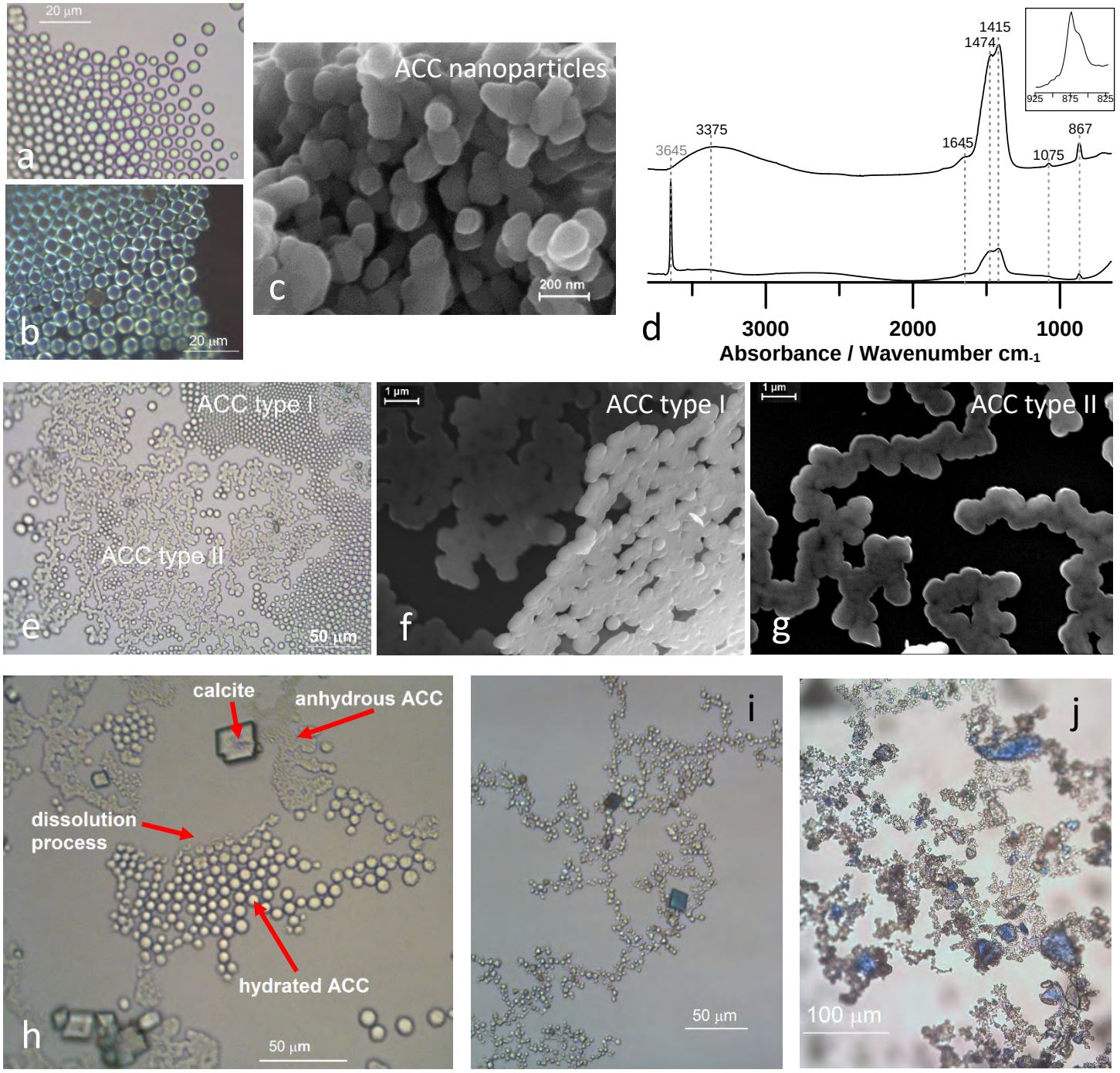
20 µm
a
b
20 µm
ACC nanoparticles
c
200 nm
1415
1474
3375
3645
1645
867
1075
925
875
825
d
3000
2000
1000
Absorbance / Wavenumber cm-1
ACC type I
ACC type II
e
50 µm
1 µm
ACC type I
f
1 µm
ACC type II
g
calcite
anhydrous ACC
dissolution process
hydrated ACC
h
50 µm
i
50 µm
j
100 µm

Figure 1

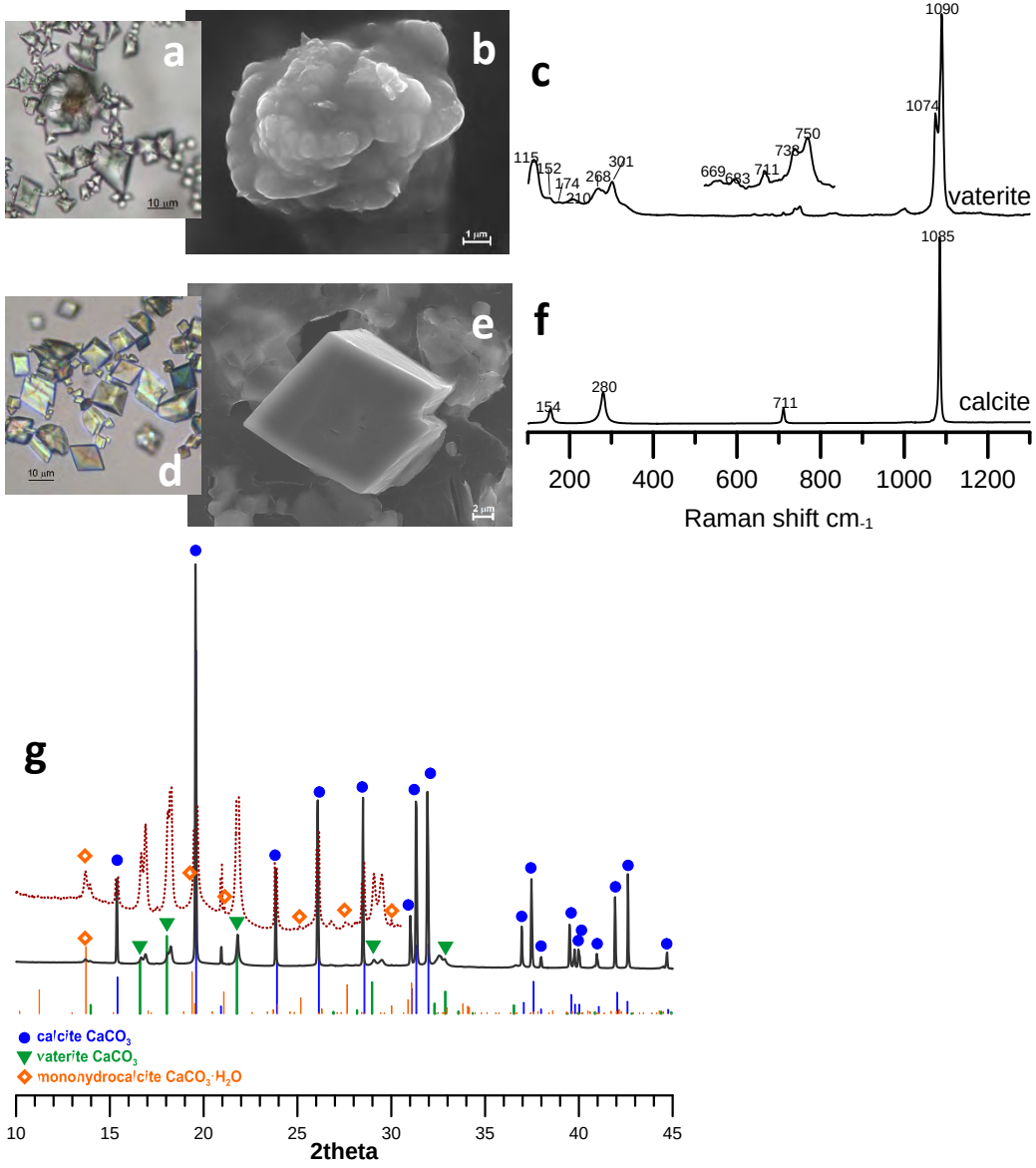
a
10 μm
b
1 μm
c
1090
1074
750
738
711
669
683
301
268
174
210
152
115
vaterite
d
10 μm
e
2 μm
f
1085
280
154
711
calcite
200
400
600
800
1000
1200
Raman shift cm-1
g
calcite CaCO3
vaterite CaCO3
mononydrocalcite CaCO3·H2O
10
15
20
25
30
35
40
45
2theta

Figure 2.

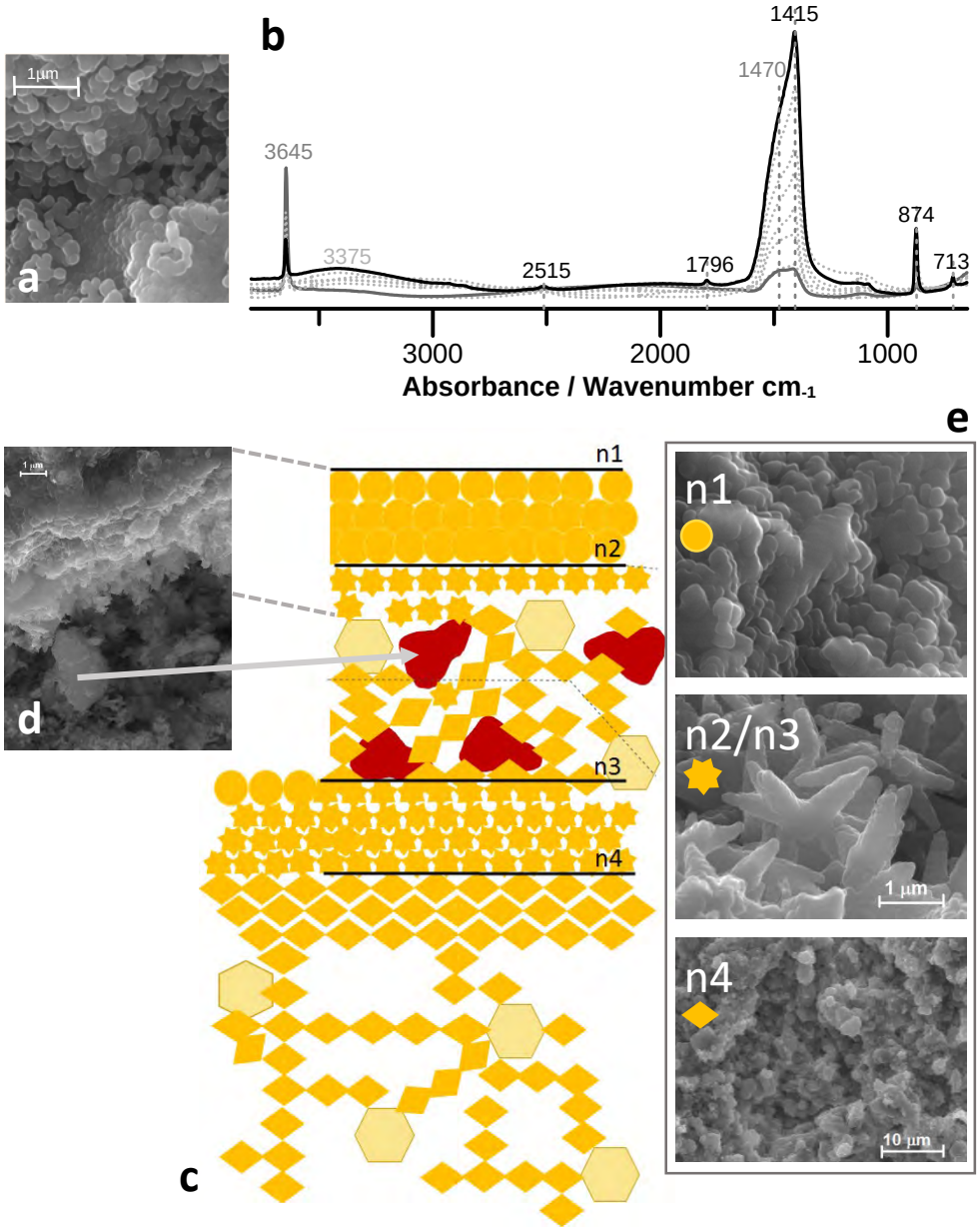
a
1µm
b
1415
1470
3645
874
3375
2515
1796
713
3000
2000
1000
Absorbance / Wavenumber cm-1
c
n1
n2
n3
n4
d
e
n1
n2/n3
1 µm
n4
10 µm

Figure 3.

Figure 4.

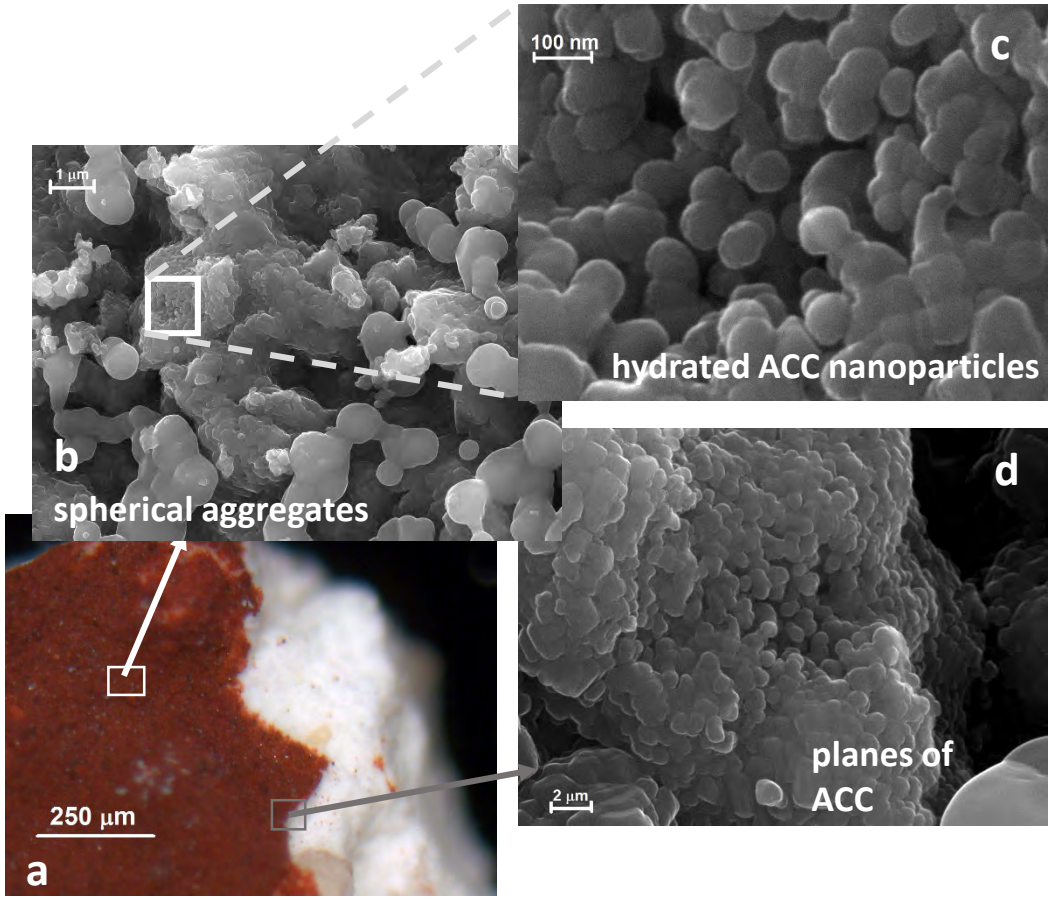
100 nm
c
hydrated ACC nanoparticles
1 μm
b
spherical aggregates
d
planes of
ACC
2 μm
250 μm
a